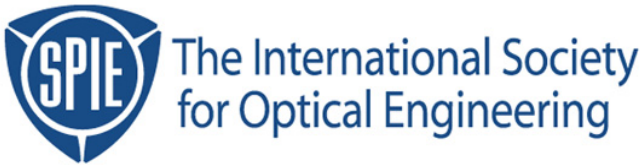

This paper was published in the proceedings of
Emerging Lithographic Technologies IV, SPIE Vol. 3997, pp. 245-254.
It is made available as an electronic reprint with permission of SPIE.

Modeling of Projection Electron Lithography

Chris A. Mack
FINLE Technologies, A Division of KLA-Tencor
8834 N. Capital of Texas Hwy, Suite 301, Austin TX 78759
chris_mack@finle.com

Abstract

Projection Electron Lithography (PEL) has recently become a leading candidate for the next generation of lithography systems after the successful demonstration of SCAPEL by Lucent Technologies and PREVAIL by IBM. These systems use a scattering membrane mask followed by a lens with limited angular acceptance range to form an image of the mask when illuminated by high energy electrons. This paper presents an initial modeling system for such types of projection electron lithography systems. Monte Carlo modeling of electron scattering within the mask structure creates an effective mask "diffraction" pattern, to borrow the standard optical terminology. A cutoff of this scattered pattern by the imaging "lens" provides an electron energy distribution striking the wafer. This distribution is then convolved with a "point spread function", the results of a Monte Carlo scattering calculation of a point beam of electrons striking the resist coated substrate and including the effects of beam blur. Resist exposure and development models from standard electron beam lithography simulation are used to simulate the final three-dimensional resist profile.

Keywords: Projection electron lithography, electron beam lithography, lithography simulation, ProBEAM/3D

I. Introduction

Electron beam lithography continues to play a vital role in semiconductor and nano technology. Current and future demands on the mask making process require tight control over every aspect of the electron beam lithography process. In addition, direct write raster and shaped beam lithographies continue to look promising for research and possibly future manufacturing. Recently, projection electron beam systems such as SCALPEL from Lucent Technologies and PREVAIL from IBM have opened the possibility of projection imaging with electrons for sub 100nm manufacturing.

Lithography modeling has proven an invaluable tool in the use and development of optical lithography over the years. In many examples of advances in lithographic technology, such as off-axis illumination, phase shifting mask design, and optical proximity correction, simulation has been used as a driver for innovation. Likewise, the development and implementation of next generation lithography technologies, such as projection electron lithography, would benefit greatly from the availability of high quality, accurate simulation tools.

This paper will show how the three-dimensional electron beam lithography simulator ProBEAM/3D [1-6] has been expanded to include the modeling of projection electron lithography (PEL). Beginning with standard Monte Carlo techniques to calculate the "point spread" electron energy distribution with a resist film, the addition of beam blur creates the energy distribution due to a minimum "spot" exposure. Convolution of this spot with the transmission function of the scattering mask/lens combination produces the electron image in the resist. Well known models of resist exposure and development chemistry are then applied. Both conventional and chemically amplified resists can be simulated. The combination of the individual parts yields a comprehensive model able to predict three-dimensional resist profiles for a wide range of projection electron beam lithography tools and resist processes.

II. Structure of the Model

The overall electron beam simulation package is structured into a set of modular components, the purpose of which is to promote the reuse of simulation results. The first module, the Monte Carlo calculations, predicts the interaction of an electron of a given energy with a given resist/substrate film stack. The result is independent of the details of the actual electron beam spot size and the pattern to be written. Thus, the output of the Monte Carlo module can be saved and reused whenever the beam energy and film stack are the same. A library of common energies and film stacks can be built up over time.

The second module, called Pixel Generation, takes the output of the Monte Carlo module and combines it with the details of the electron beam blur to create a "spot" or "pixel" image in the resist. The result is the energy distribution within the resist for an electron beam of a given beam energy with a given amount of Gaussian blur and for a given film stack.

Once a spot image in the resist has been calculated, this spot can be convolved with the mask pattern to produce the image in the resist. The scattering behavior of the mask followed by the angular limitations of the imaging lens results in an effective transmission function of the mask. It is this transmission function which is then convolved with the beam-blurred spot image in the resist. The result is a three-dimensional image of deposited energy within the resist. This image then exposes the resist material, which can be positive or negative acting, conventional or chemically amplified. A post-exposure bake can be used to diffuse (and possibly react) chemical species in the exposed resist, followed by a three-dimensional development to give the final resist profile. The general sequence of events is pictured in Figure 1.

The following sections will describe each step in the modeling sequence in more detail.

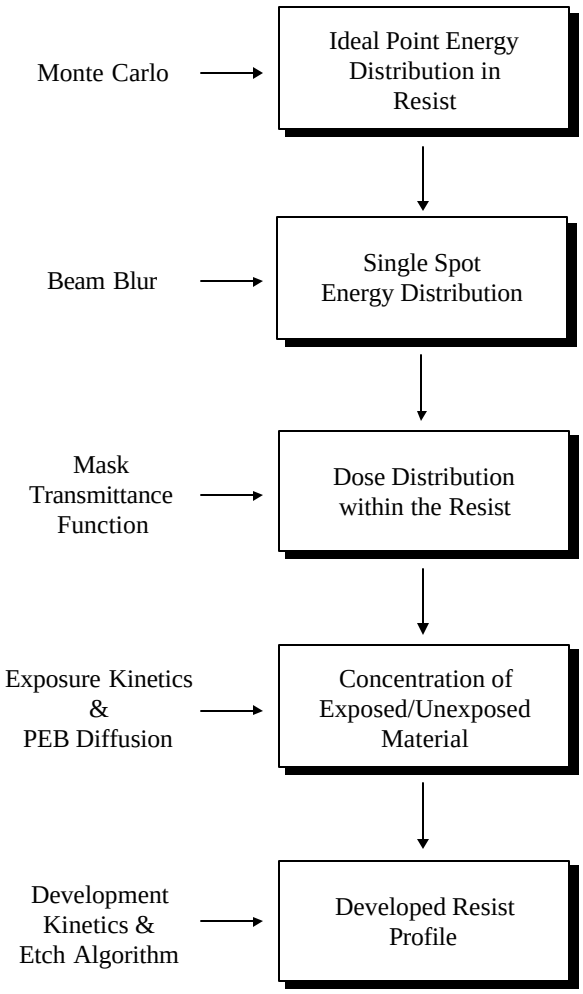

Figure 1. Flow diagram of the ProBEAM/3D electron beam lithography simulator for projection electron beam imaging.

2.1 Monte Carlo Calculations

The Monte Carlo calculations use standard techniques that have been extensively reported in the literature [7]. An electron scatters off nuclei in a pseudo-random fashion. The distance between collisions follows Poisson statistics using a mean free path based on the scattering cross-section of the nuclei. The energy loss due to a scattering event is calculated by the Bethe energy loss formula. The "continuous slowing-down approximation" is used to spread this energy over the length traveled. Many "simulated" electrons (typically 100,000 – 1,000,000) are used to bombard the material and an average energy deposited per electron as a function of position in the solid is determined. For higher beam energies, more electrons are typically required to get good statistics.

Results of the Monte Carlo calculations are shown in Figures 2 and 3, using conditions pertinent to current projection electron beam imaging. Figure 2 shows the electron trajectories of 100 electrons in

300nm of resist on silicon for 100KeV electron energy. The deposited energy distribution in resist resulting from these trajectories is shown in Figure 3 (using 500,000 electrons to get good statistics), where the physically-based assumption of radial symmetry is used to collect deposited energy in radial, logarithmically spaced bins.

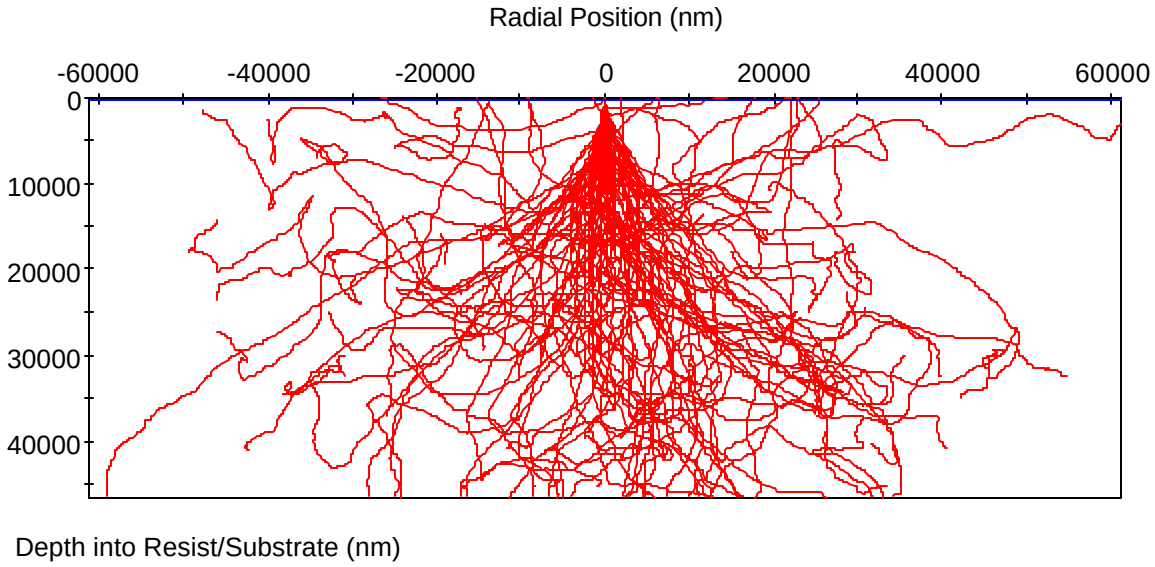

Figure 2. Electron trajectories of 100 electrons in 300nm of resist on silicon for 100KeV electron energy.

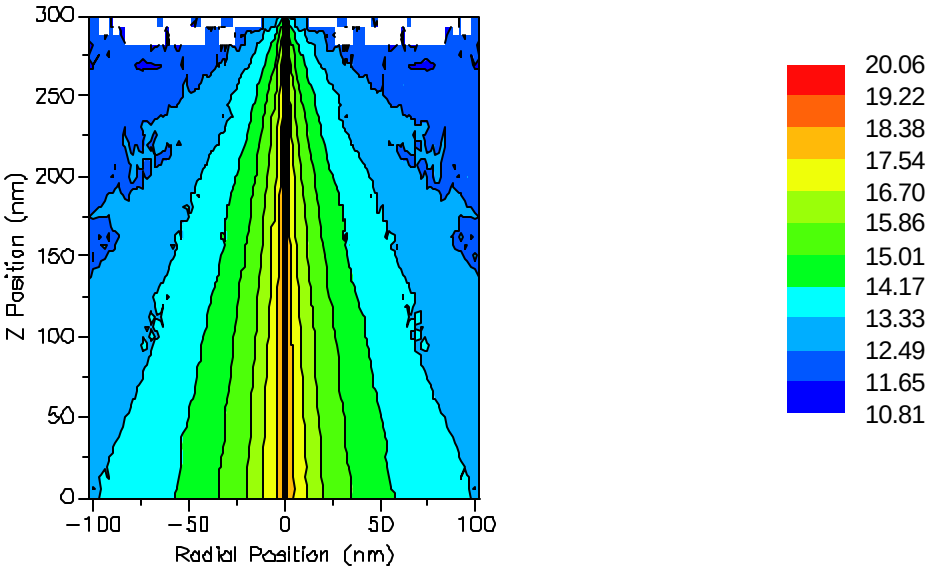

Figure 3. The deposited energy distribution in resist resulting from an ideal 100KeV beam (using 500,000 electrons in the Monte Carlo calculations, 300nm resist on silicon). Contours show log(eV/cm^3/electron).

2.2 Beam Blur

The final result of the Monte Carlo calculation is the average energy distribution of a single electron of a given initial energy normally incident on the material/film stack at a single point. However, in any real exposure system Coulomb-Coulomb interactions of the electrons produce a current-dependent beam blur. In general, this blur can be well approximated by a Gaussian-shaped spot of a certain full width at half maximum (FWHM). The Monte Carlo result can be used to generate a "spot", the deposited energy for an average electron including the effects of beam blur. The pixel is generated as the convolution of the Monte Carlo point energy distribution with the beam shape. Figure 4 shows example pixels, using the Monte Carlo results of Figure 3, for Gaussian shaped beam blurs of 20nm and 40nm FWHM and for a beam energy of 100KeV incident on 300nm of resist on silicon.

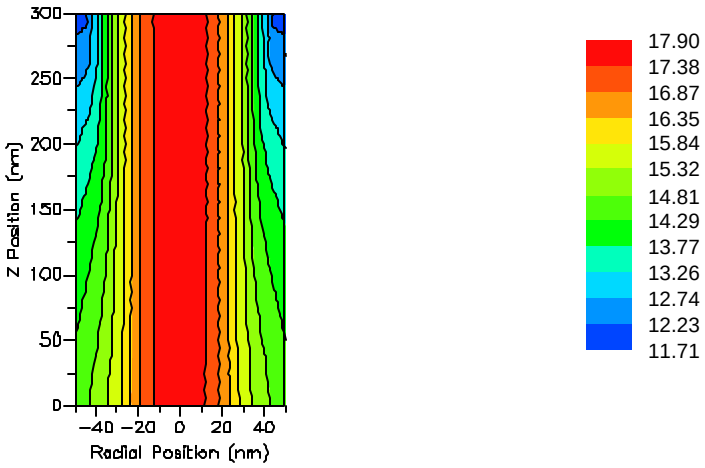

(a)

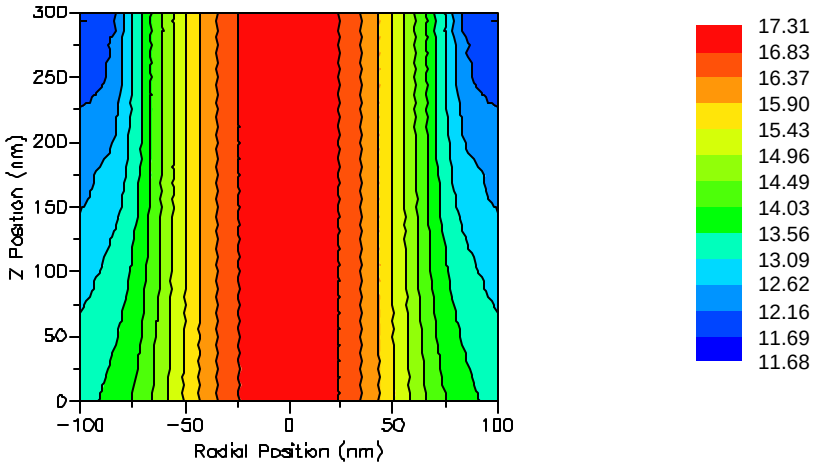

(b)

Figure 4. The convolution of a Gaussian beam blur with the Monte Carlo results of deposited energy for an ideal spot produces a real "spot" image in the resist for FWHM beam blurs of a) 20 nm, and b) 40nm. Contours show log(eV/cm^3/electron).

2.3 Mask Transmittance and Projection Imaging

Although the exact configuration of future SCALPEL or other PEL masks is not yet completely determined, the basic mask consists of a SiN_x membrane of thickness 100 – 150nm for the "clear" or high non-scattered transmittance regions, with a metal film stack of 5 – 10nm of chrome over 25 – 50nm of tungsten coated on this membrane for the "dark" or low non-scattered transmittance regions [8,9]. To understand how these structures transmit 100KeV electrons, the Monte Carlo simulator portion of ProBEAM/3D was modified to collect the angular distribution of electrons emanating from the thin film. Monte Carlo runs of 500,000 electrons were executed for different thin films surrounded by air. The angle of the electrons exiting the film were determined and collected in 0.1 degree (1.7 mrad) bins to determine the frequency distribution of electrons as a function of exit angle. Two structures were simulated: a) 150nm Si_3N_4, and b) 5nm Cr/25nm W/150nm Si_3N_4. The results are shown in Figure 5.

The data show two very important effects. First, the 150nm Si_3N_4 membrane transmits 32% of the incident electrons with essentially no scattering, while the 5nm Cr/25nm W/150nm Si_3N_4 film stack transmits 6.5% of the incident electrons without scattering. Second, the scatterer film stack spreads the larger number of scattered electrons over a wider range of angles. Interestingly, the probability density function described by the given Monte Carlo data can be very well fit by the following model:

$$P(q) = a_0 d(q) + a_1 \sin q \, e^{-(\sin q / \sin q_o)^m} \qquad (1)$$

where $P(\theta)$ is the probability that an electron will be scattered with an angle between θ and $\theta+d\theta$ and $\delta(\theta)$ is the Dirac delta function. The term a_0 represents the fraction of electrons that are not scattered.

From the data shown in Figure 5 along with two other cases, the scatter model parameters from equation (1) are given in Table I. In addition, the cases of a 100nm Si_3N_4 membrane and a 10nm Cr/50nm W/100nm Si_3N_4 film stack were also calculated. Given the numerical aperture of the projection optical system (the sine of the maximum half angle of scattered electrons that can pass through the projection system) on the mask side, the maximum scattered angle that is transmitted to the wafer is known. (Note that for the small angles used here, $\sin\theta \approx \theta$.) For example, if the numerical aperture is 5 mrad (0.3 degrees), the unscattered portion of the transmittance (the a_0 term in equation (1)) will dominate the portion of the mask transmittance that actually makes it to the wafer. Thus, for the data given here for the thick membrane/thin scatterer, the mask transmittance function can be approximated as a relative membrane transmittance of 1.0 and a "dark" scatterer transmittance of 0.20. Since the mask assumed here used the maximum membrane thickness and the minimum scatterer thickness, this 5:1 mask contrast is a worst case scenario. On the other hand, the thin membrane with the thick scatterer layer produces a mask contrast of 23:1. It is likely that actual SCALPEL masks will fall between these two extremes. It is hoped that

comparisons between actual measured mask transmittance functions and these simulated results can be used to fine-tune the high energy scattering parameters used in the Monte Carlo calculations.

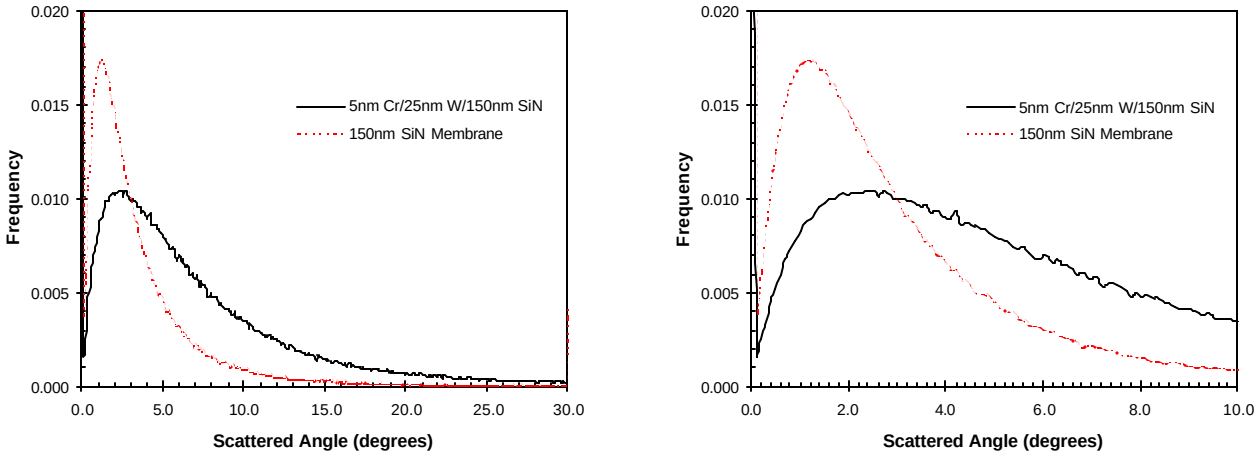

Figure 5. Comparison of the scattered electron angular distribution for 150nm SiN membrane and for the scatter film stack of 5nm Cr/25nm W/150nm SiN. Two different x-axis scales are shown for better comparison. Not shown on the graph is the fact that the membrane transmits 32% of the incident electrons with no scattering and the scatter film stack transmits 6.5% of the incident electrons without scattering.

Table I. Fit of the scatter model to the Monte Carlo data.

Film	a_0	a_1	q_o	m
100nm Si_3N_4	0.463	2.66	0.83	0.81
150nm Si_3N_4	0.321	2.97	0.83	0.78
5nm Cr/25nm W/150nm Si_3N_4	0.065	1.04	1.41	0.70
10nm Cr/50nm W/100nm Si_3N_4	0.020	0.374	3.03	0.82

Once the anglularly limited transmittance function of the membrance mask is known, convolution of this transmittance function with the beam blurred single spot energy distribution in the resist produces the actual image in resist: the energy distribution in resist at the end of exposure.

2.4 Resist Exposure and Development

Resist exposure and development models have been borrowed from optical lithography simulation [10-13] and applied to e-beam lithography [2,3]. The Dill exposure model [10,11] is based on a first order chemical reaction of some radiation-sensitive species of relative concentration m.

$$\frac{dm}{dE} = -Cm \tag{2}$$

where E is the e-beam deposited exposure dose at some point in the resist (in J/cm^3) and C is the exposure rate constant (with units of 1/dose). The solution to this rate equation is a simple exponential.

$$m = e^{-CE} \tag{3}$$

The use of equations (2) and (3) differs from optical lithography simulation in that the e-beam case uses deposited energy per unit volume and the optical lithography case use energy per unit area. The difference is straightforward since the optical absorption coefficient of the resist relates energy per unit area to deposited energy per unit volume [12]. Thus, the exposure rate constant C for electron beam exposure is roughly equivalent to the optical C divided by the resist optical absorption coefficient α. As an order of magnitude analysis, typical optical resists exhibit $C \sim 0.02\text{cm}^2/\text{mJ}$ and $\alpha \sim 0.5\mu\text{m}^{-1}$. Thus, the e-beam equivalent value of C (for the same effective resist sensitivity) would be about $0.004\text{cm}^3/\text{J}$.

The relative sensitizer concentration m (or the reaction product of concentration 1-m) then controls the development process. The Mack kinetic model [13], the enhanced kinetic model [14], or some equivalent model can then be applied. The standard Mack model takes the form (for a positive resist)

$$r = r_{\max}\frac{(a+1)(1-m)^n}{a+(1-m)^n} + r_{\min} \tag{4}$$

where r_{max} is the maximum development rate for completely exposed resist, r_{min} is the minimum development rate for completely unexposed resist, n is the dissolution selectivity (proportional to the resist contrast), and a is a simplifying constant given by

$$a = \frac{(n+1)}{(n-1)}\left(1-m_{TH}\right)^n \tag{5}$$

where m_{TH} is called the threshold value of m. For a negative resist, the terms 1-m in equations (4) and (5) are replaced by m.

Chemically amplified resists can also be simulated using reaction-diffusion models developed for optical lithography [15,16]. In fact, many chemically amplified resists developed for deep-UV lithography are being extensively used as the next generation of high resolution electron beam resists.

III. Conclusions

The importance of lithography simulation as a research, development and manufacturing tool continues to grow. Likewise, the quick approach of sub 100nm semiconductor manufacturing requirements has made the development of next generation lithography technologies such as projection electron lithography even more critical. This paper presents a new tool for studying the intricacies of projection electron lithography as an extension to the ProBEAM/3D modeling system. Monte Carlo simulations are combined with a beam blur shape to generate a single "spot" energy distribution. This spot is then convolved with the mask transmittance function (itself generated by Monte Carlo calculations). The resulting dose pattern is used to expose and develop a resist to form a three-dimensional resist pattern.

Acknowledgments

The author wishes to thank Scott Mackay of SEMATECH for support and guidance.

References

1. C. A. Mack, "Three-Dimensional Electron Beam Lithography Simulation," *Emerging Lithographic Technologies, Proc.*, SPIE Vol. 3048 (1997) pp. 76-88.
2. C. A. Mack, "Electron Beam Lithography Simulation for Mask Making, Part I," *17th Annual BACUS Symposium on Photomask Technology and Management*, SPIE Vol. 3236 (1997) pp. 216-227.
3. C. Sauer, D. Alexander and C. A. Mack, "Electron Beam Lithography Simulation for Mask Making, Part II: Comparison of the Lithographic Performance of PBS and EBR900-M1," *17th Annual BACUS Symposium on Photomask Technology and Management*, SPIE Vol. 3236 (1997) pp. 413-423.
4. C. A. Mack, "Electron Beam Lithography Simulation for Mask Making, Part III: Effect of Spot Size, Address Grid and Raster Writing Strategies on Lithography Performance with PBS and ZEP-7000" *18th Annual BACUS Symposium on Photomask Technology and Management*, SPIE Vol. 3546 (1998).
5. C. Sauer and C. A. Mack, "Electron Beam Lithography Simulation for Mask Making, Part IV: Effect of Resist Contrast on Isofocal Dose," *Photomask and X-Ray Mask Technology VI, Proc.*, SPIE Vol. 3748 (1999) pp. 27-40.
6. C. A. Mack and C. Sauer, "Electron Beam Lithography Simulation for Mask Making, Part V: Impact of GHOST proximity effect correction on process window," *19th Annual BACUS Symposium on Photomask Technology and Management, Proc*., SPIE Vol. 3873 (1999) pp. 2-20.
7. R. J. Hawryluk, A. M. Hawryluk, and H. I Smith, "Energy Dissipation in a Thin Polymer Film by Electron Beam Scattering," *Journal of Applied Physics*, Vol. 45, No. 6 (June, 1974) pp. 2551-2566.
8. J. A. Liddle, et al., "Proximity Effect Correction in Electron Beam Lithography (Scattering with Angular Limitation Projection Electron-Beam Lithography)", *Japanese Journal of Applied Physics*, Vol. 34, No. 12B (Dec. 1995) pp. 6672-6678.
9. M.M. Mkrtchyan, et al., "Electron Scattering and Transmission through SCALPEL Masks", *Journal of Vacuum Science and Technology B*, Vol. 16, No. 6 (Nov/Dec. 1998) pp. 3385-3391.

10. F. H. Dill, W. P. Hornberger, P. S. Hauge, and J. M. Shaw, "Characterization of Positive Photoresist," *IEEE Trans. Electron Dev.*, ED-22, No. 7, (1975) pp. 445-452, and *Kodak Microelectronics Seminar Interface '74* (1974) pp. 44-54.

11. C. A. Mack, "Absorption and Exposure in Positive Photoresist," *Applied Optics*, Vol. 27, No. 23 (1 Dec. 1988) pp. 4913-4919.

12. A. R. Neureuther, M. Zuniga, and N. Rau, "Modeling of the Patterning Process with Chemically-Amplified Resists," *Microprocess and Nanotechnology '97, Proc*. (1997).

13. C. A. Mack, "Development of Positive Photoresist," *Jour. Electrochemical Society*, Vol. 134, No. 1 (Jan. 1987) pp. 148-152.

14. C. A. Mack, "New Kinetic Model for Resist Dissolution," *Jour. Electrochemical Society*, Vol. 139, No. 4 (Apr. 1992) pp. L35-L37.

15. C. A. Mack, "Lithographic Effects of Acid Diffusion in Chemically Amplified Resists," *OCG Microlithography Seminar Interface '95, Proc.*, (1995) pp. 217-228, and Microelectronics Technology: Polymers for Advanced Imaging and Packaging, ACS Symposium Series 614, E. Reichmanis, C. Ober, S. MacDonald, T. Iwayanagi, and T. Nishikubo, eds., ACS Press (Washington: 1995) pp. 56-68.

16. J. S. Petersen, C. A. Mack, J. Sturtevant, J. D. Myers and D. A. Miller, "Non-constant Diffusion Coefficients: Short Description of Modeling and Comparison to Experimental Results," *Advances in Resist Technology and Processing XII, Proc.*, SPIE Vol. 2438 (1995) pp. 167-180.